J Mater Sci (2009) 44:463–468
DOI 10.1007/s10853-008-3091-2

Mechanical property under high dynamic loading and microstructure evaluation of a TiB_2 particle-reinforced stainless steel

H. Nahme · E. Lach · A. Tarrant

Received: 25 August 2008 / Accepted: 28 October 2008 / Published online: 23 November 2008

Abstract The incorporation of low density, high modulus ceramic particles into a steel matrix is a potential route to improve the mechanical performance of steels. A powder metallurgy, mechanical blending route has been adopted to produce a homogeneous distribution of TiB2 particles in a 316L stainless steel matrix. The resulting composite showed large increases in both the compression and the tensile strength when compared to the unreinforced alloy. The compression strength was measured under both quasistatic and dynamic conditions. Tensile strength was measured only under quasistatic conditions. Dynamic compression tests were performed at temperatures of 200 and 400 °C. Metallographic investigations have been performed on the specimen in the initial status and after a deformation. Fracture surfaces were studied in a scanning electron microscope to allow more detailed assessment of fracture mechanisms.

Introduction

Steels that are strong in both tension and compression are of great interest for many engineering applications, for example aerospace, automotive components and also lightweight armour. However, in many cases high-strength steels cannot be applied because of their poor toughness due to the competition between strength and toughness. Due to their face centre cubic crystal structure, austenitic steels are tough, but (compared to ferritic steels) show only moderate strength.

A powerful method to improve the strength and toughness of austenitic steels is to use nitrogen as an alloying element [1]. Uggowitzer [2] reports on nitrogen-alloyed austenitic steel containing 0.6 wt.% N in solid solution, which shows an extremely high strength of 3,380 MPa. This strength can be achieved by a combination of solid solution hardening, grain-boundary hardening, dislocation strengthening and strain ageing. The very high tensile strength could be realised only on thin wires (diameter 1 mm).

Another powerful route to improve the strength of austenitic steels is to incorporate low density, high stiffness ceramic particles in the matrix alloy. In this work, the 316L stainless steel has been chosen as matrix alloy and has been reinforced with fine-grained ($d < 10$ μm) TiB_2 particulate reinforcement. The necessity of highly mobile armoured vehicles requires lightweight materials, but high strength steel with reduced density and enhanced strength also offers design benefits for lightweight armour.

Materials

Manufacturing

The MMC (Metal Matrix Composite) used in this work was manufactured by Aerospace Metal Composites Limited using a powder metallurgy process. The powder raw

H. Nahme
Ernst-Mach-Institute, EMI, Freiburg, Germany
e-mail: nahme@emi.fhg.de

E. Lach (✉)
French-German Research Institute of Saint Louis, ISL,
Saint Louis, France
e-mail: lach@isl.tm.fr; elach@gmx.de

A. Tarrant
Aerospace Metal Composites Limited, AMC, Farnborough, UK
e-mail: andrew.tarrant@amc-mmc.co.uk

Table 1 Nominal chemical composition of 316L in wt.%

C	Cr	Ni	Mo	Mn	Si
0.03	17.5	12	2.5	2	1

Table 2 Provisional data for Extruded 316L/15 vol.% TiB_2 [11]

Ultimate strength (Mpa)	0.2% yield strength (Mpa)	Strain to failure (%)	Density (g cm^{-3})	Specific stiffness (GPa)
885	495	11	7.4	29

materials were austenitic stainless steel and fine-grained ($d < 10$ μm) titanium diboride (TiB_2). Typical D50 grain size for the TiB2 particles are 4 to 5 microns. Table 1 shows the chemical composition of the 316L matrix powder. The ceramic was blended and mechanically alloyed with the steel matrix at a volume fraction of 15%. The powders were encapsulated and consolidated using hot isostatic pressing [3]. Typical properties for the 316L/15 vol.% TiB_2 are shown in Table 2.

Microstructure

The microstructure of the MMC is shown in Fig. 1. It shows that the particle distribution is relatively homogeneous, but shows some regions that are free of particles (bright areas).

TiB_2 is selected because of its compatibility and stability with steel matrices. However, there are some reactions that occur probably as a result of impurities present in the TiB_2 particles. The grey phases (arrow in Fig. 1) in the microstructure are Cr/Mo-rich phases, which appear especially when fine-grained TiB_2 ($d < 1.5$ μm) is used. This may be due to the surface area and/or purity of the TiB_2. However, it is not finally assured whether this phase is a boride or a carbide.

Experimental methods

Quasistatic and dynamic tensile and compression tests

Quasistatic tensile and compression tests were performed on a universal testing machine at strain rates of about 5×10^{-3} s^{-1}. To determine the dynamic compression behaviour of the particle-reinforced 316L alloy at strain rates ranging from 10^{-3} s^{-1} to 5×10^{3} s^{-1}, a split-Hopkinson-pressure-bar (SHPB) set-up has been used [4, 5]. The tensile tests were performed on specimens with a gauge diameter of 3 mm to 3.5 mm and a gauge length of 15 mm. The compression tests were performed with specimen of 6 mm to 10 mm in diameter and 4 mm to 8 mm in lengths resulting in L/D ratios of 0.67 to 0.83.

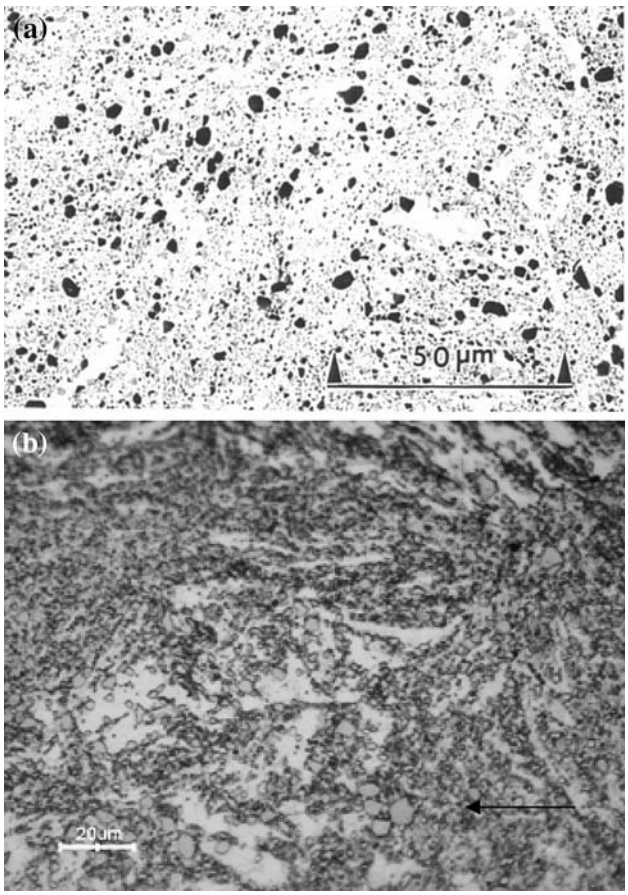

Fig. 1 **a** and **b** The initial microstructure of the investigated MMC

Plate impact

To determine the high strain rate properties of TiB_2-reinforced material, the plate impact technique in combination with a VISAR has been used, frequently described in detail elsewhere [6].

Plane parallel C45 steel plates of 3 mm thickness have been accelerated by means of a compressed air or powder gun to impact velocities of $200 < v < 900$ m/s. The 316L TiB_2 plates being tested were of thicknesses of 5 mm and 50 mm in diameter.

The impact of a projectile plate onto a sample plate generates pressure stress waves propagating into both plates causing compression stress. These waves accelerate the sample material and decelerate the projectile material. When the pressure waves reach the free surfaces of both plates, they are converted to pressure release waves and are reflected back into the plate material. The superposition of these release waves inside the sample plate causes high dynamic tension stress, yielding in spallation when the

dynamic tension strength (spall strength) of the material is exceeded.

With the VISAR the velocity of the rear sample surface was monitored with a time resolution of 2 ns. From this velocity-time history dynamic properties like the Hugoniot Elastic Limit (HEL), spall strength, shock velocity and the stresses and strains achieved are determined. From these data, the shock velocity–particle velocity and stress–strain relations have been deduced.

Results

Tensile and compression tests

Figure 2 shows the results of the quasistatic tensile tests. The 0.2% yield strength and the ultimate strength are similar to the provisional data in Table 2. Only the elongation to fracture is significantly smaller and amounts to 5% compared to 11% in Table 2. However, the materials tested in this programme were in an As HIP condition where 5% elongation is to be expected. The tensile specimen with gauge diameter of 3.5 mm possesses an increased elongation to fracture. The gauge length was also 15 mm, so the increased ductility is due to the smaller L/D ratio.

A comparison of the tensile tests of both the non-reinforced and reinforced 316L reveals the advantage of the reinforcement. The 0.2% yield strength and the ultimate strength for the non-reinforced 316L steel amounts to 225 MPa and 520 MPa, respectively. A TiB_2 particle reinforcement increases these values to about 495 MPa and 885 MPa, respectively. Young's modulus is also augmented from 196 GPa to 218 GPa, but the elongation to failure is strongly decreased from 45% to about 6% for the reinforced material.

Figure 3 summarises the results of the quasistatic compression tests. Compression test specimens were cut from the hipped MMC plates using electro-discharge machining.

Subsequently, the specimens were ground to obtain smooth surfaces. Prior to testing the specimens were

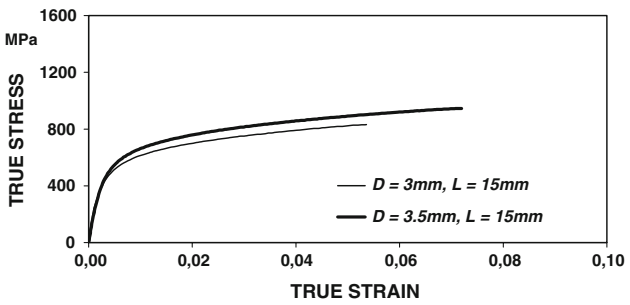

Fig. 2 Quasistatic tensile test performed on specimen with different L/D ratio. D = diameter and L = length of specimen

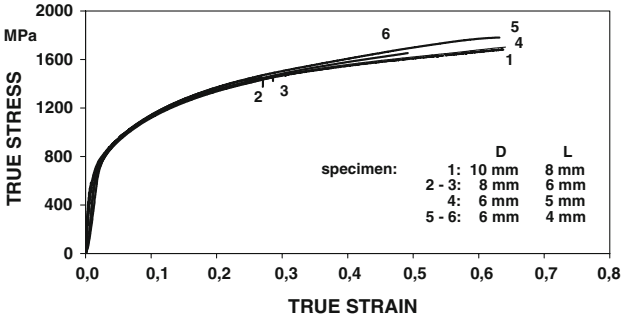

Fig. 3 Quasistatic compression test. The numbers indicate the specimen's geometry prior to compression. D = diameter and L = length of specimens

lubricated with ball bearing grease in order to reduce frictional effects.

It is obvious that the compression strength in Fig. 3 is considerably higher than the ultimate tensile strength (Fig. 2). The compression strength is twice that of the ultimate tensile strength. This phenomenon is well known from investigations on particle-reinforced Mg and Al alloys as shown for Mg-based MMC in reference [7]. A reinforcement using particles mainly increases Young's modulus and the flow stress. Particle reinforcement mainly acts as an obstacle to dislocations. Between $\varepsilon = 5\%$ and 20% the quasistatic compression flow curve has an average work hardening rate of $\Theta = d\sigma/d\varepsilon = 2{,}600$ MPa. This range is followed by a linear increase of the flow stress with strain from $\varepsilon = 20\%$ up to fracture. In this strain range of the tests a work hardening rate of $\Theta = d\sigma/d\varepsilon = 1{,}000$ MPa has been determined.

Under the condition of a compression test the hydrostatic pressure enables a very high deformation of specimen as shown in Fig. 3 compared to the tensile tests in Fig. 2. The reinforcement prevents the formation of an internal compression cone.

The variation of the quasistatic compression strength in Fig. 3 is due to different L/D ratios. Friction became important particularly for quasistatically compressed specimens having a low L/D ratio. With respect to longitudinal and radial inertia in dynamic compression tests, a L/D ratio of about 0.5 is recommended [8]. For comparison of quasistatic and dynamic compression tests, the specimen geometry has to be identical. The effect of friction on the results is decreased under the condition of a dynamic compression test as shown in reference [9].

Due to the lack of stress equilibrium at small strains during SHPB tests, flow stresses are typically evaluated at plastic strains in the range of 3 to 5%. For this reason, the stress at 5% strain replaces the 0.2% offset flow stress.

For strains $5\% < \varepsilon < 20\%$ the work hardening rate of the dynamic flow curves in Fig. 4 has been determined to be about $\Theta = d\sigma/d\varepsilon = 2{,}300$ MPa. At higher strains the

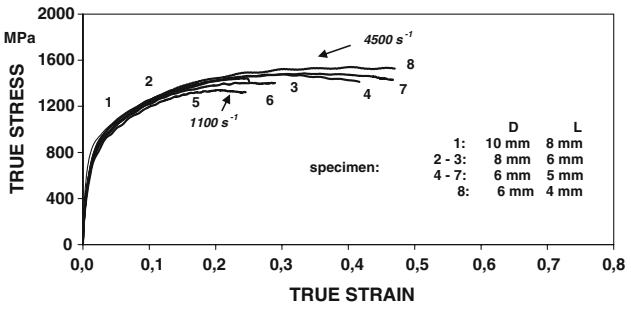

Fig. 4 Dynamic compression test

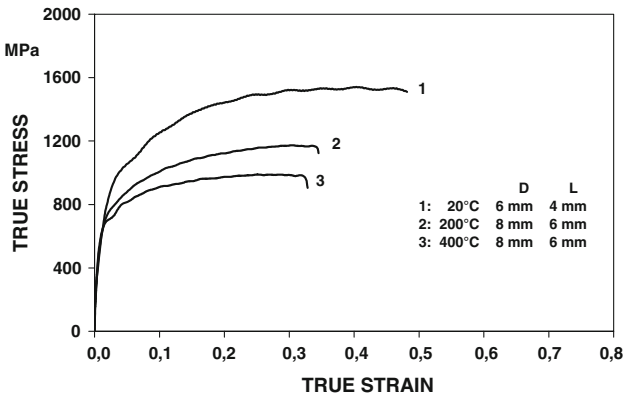

Fig. 5 Dynamic compression test at elevated temperature

work hardening rate is strongly decreased. This is due to the adiabatic nature of the dynamic compression test. The strain rate sensitivity of the investigated MMC is negligible. Higher strain rates primarily result in a higher degree of deformation. The failure by fracture of the dynamic compressed specimens occurs at nearly about 50% of deformation. This shows that the 316L-based MMC can suffer a very high dynamic loading.

Figure 5 summarises the dynamic compression tests at elevated temperature. A dynamic compression flow curve measured at room temperature is also included. An increase of the test temperature from room temperature to 200 °C decreases the dynamic compression strength relatively strongly from 1,600 MPa to 1,200 MPa. A further increase of the test temperature to 400 °C causes a smaller decrease of the compression strength to 1,000 MPa. The work hardening rate decreases also with increasing temperature.

Plate impact

In Fig. 6 the velocity–time histories of the plate impact tests are shown. Compared to curves of homogeneous materials the velocity histories exhibit nearly no distinct Hugoniot Elastic Limit (HEL). A reason for this behaviour may be the inhomogeneous internal structure of the samples causing multiple reflections of the elastic wave

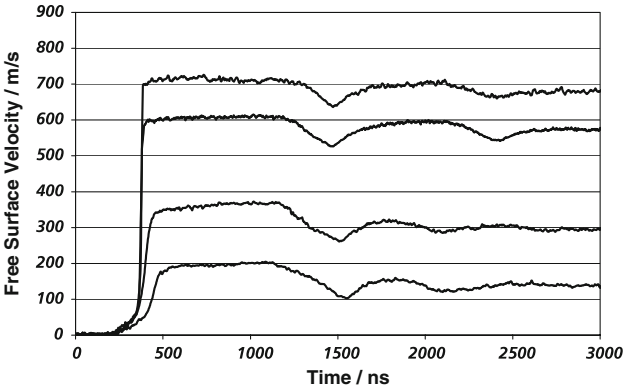

Fig. 6 Velocity-time histories for 316L-TiB_2 for 200 m/s, 382 m/s, 625 m/s and 886 m/s impact velocity

propagating through the sample with the longitudinal sound velocity. From a differential reduction of the plate impact data a value of 2,000 MPa for the 0.2% yield point can be determined. To compare this value determined under 3D stress conditions to the values measured under the 1D conditions of the quasistatic tests, a factor of $(1 - 2\upsilon)/(1 - \upsilon)$ has to be taken into account with the Poison ratio υ of 0.3, yielding a value of 1,150 MPa. This seems to be considerably higher than the corresponding value at quasistatic compression.

The first slow rise of the rear surface velocity is followed by the velocity increase due to the plastic wave front. From the longitudinal sound speed the arrival time of the plastic wave front the shock velocity has been deduced using standard procedures [6]. The U_s–u_p correlation is shown in Fig. 7 with a linear fit of $U_s = 0.99u_p + 5{,}358$ m/s (5,358 m/s represents the bulk sound velocity).

From the velocity histories it can be seen that an impact at 886 m/s only results in a maximum free surface velocity of around 700 m/s. This is typical for martensitic steel, which undergoes a phase transition from the bcc to the fcc crystal structure at high stresses caused by impact velocities higher than 700 m/s for an impact of a steel projectile onto a steel target. As a consequence, the shock velocity reaches a maximum value for martensitic steels as well. The shock velocity starts to rise again only at very high

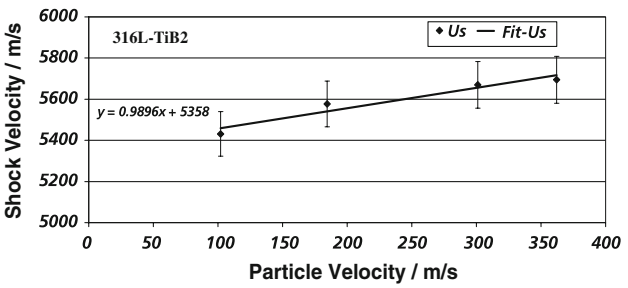

Fig. 7 Shock velocity–particle velocity diagram for 316L-TiB_2

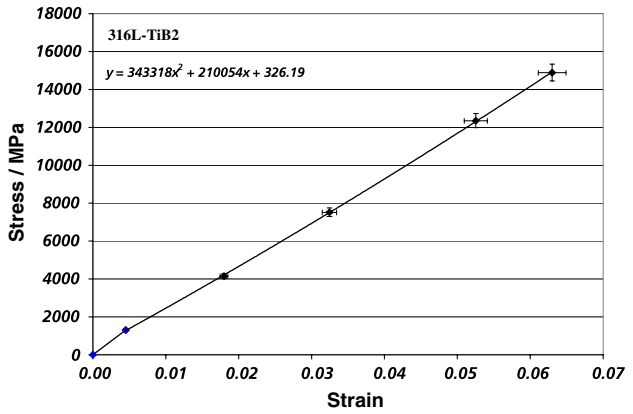

Fig. 8 Stress-strain diagram for 316L-TiB_2, each data point represents the stress-strain value of a single experiment

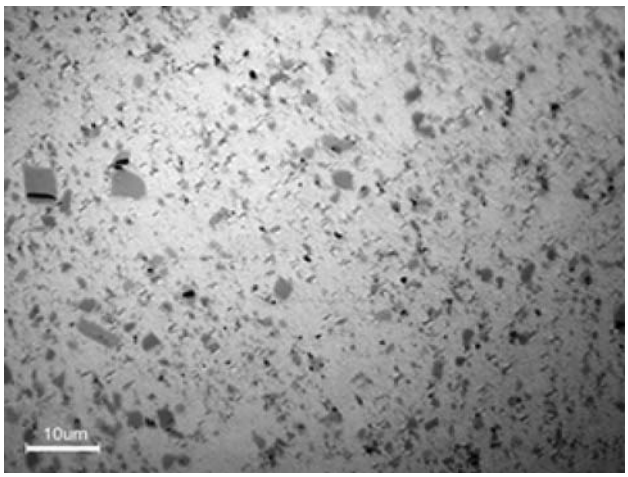

Fig. 9 Micrograph of a dynamically compressed specimen

impact velocities. Due to its fcc crystal structure the 316L matrix material should not show this effect. From the results achieved so far, this effect cannot be explained.

An explanation is possible by taking the dislocation dynamics into consideration. Orowan [10] described a model of the dispersion mechanism of particle-reinforced metallic materials. The particles impede the motion of the dislocations to a degree which depends on the particle size and separation. The dislocation line then encircles the particles. Because this process retards the movement of dislocations, it affects the shock velocity.

The plastic wave stresses the material to the Hugoniot stress, which in Fig. 6 is represented by the maximum velocity achieved. From the velocities the stresses and strains have been calculated yielding a stress-strain curve shown in Fig. 8.

When the spall process has occurred, the tension release wave emanating from the spall plane and propagating towards the rear surface of the sample causes a velocity decrease. From the amount of velocity decrease around 1,500 ns in Fig. 6 the spall strength was deduced [6]. The values achieved are 1,950 MPa $< \sigma_{spall} <$ 2,630 MPa and seem to decrease with increasing impact velocity and thus increasing Hugoniot stress.

To compare these values to the values determined quasistatically the 3D-1D transformation has to be taken into account. Thus yield strengths of 1,100 MPa $<$ Y $<$ 1,500 MPa have been reached at strain rates in the range of $d\varepsilon/dt = 10^4\ s^{-1}$ which is significantly higher than the ultimate strength of 885 MPa measured at quasistatic conditions.

Metallography and scanning electron microscopy

Figure 9 shows the microstructure of the 316L MMC after a dynamic compression test. The specimen was dynamically compressed up to fracture. Microcracking occurs in the brittle TiB_2 particle, but no decohesion between matrix and reinforcement particle could be found. The formation of an internal compression cone is prevented by the reinforcement particles. Hence, the plastic deformation occurs locally around the TiB_2 particles. Metallographic investigation revealed that no adiabatic shearbanding occurred.

In Fig. 10a, a dynamically compressed specimen with two major cracks is shown. The cracks are initiated at the maximum diameter and were propagating into the specimen at an angle of 45°.

Details from the fracture surface are shown in Fig. 10b. The surface is characterized by elongated dimples and secondary microcracks. Elongated dimples refer to shear fracture. On the surface some inclusions can be seen. It can be assumed that these are the reinforcement particles.

The SEM fractograph in Fig. 11 shows the fracture surface of the plate subjected to a plate impact. The fracture surface is characterised by TiB_2 particles showing transgranular cleavage fracture and colonies of very small dimples. The small size of the dimples is due to a very high strain rate as it occurs during a very rapid crack propagation caused by shock wave loading.

Conclusions

The matrix alloy of the investigated MMC possesses only moderate strength compared to ferritic steels due its face centre cubic structure. The incorporation of fine-grained TiB_2 particles into the alloy is a potential route to improve the mechanical performance of austenitic steels. Stiffness is also increased and density is reduced to 7.4 g/cc.

The MMC was manufactured using a powder metallurgy process. TiB_2 is selected because of its compatibility and stability with steel matrices. However, a Cr/Mo-rich phase appears in the microstructure when fine-grained TiB_2 is

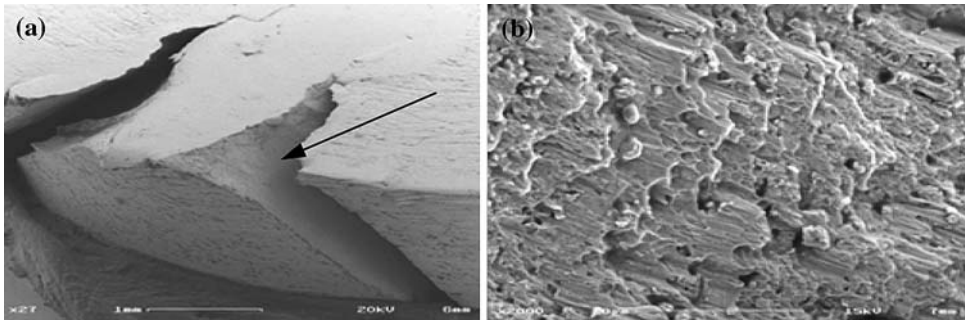

Fig. 10 **a** SEM fractograph of a dynamically compressed specimen with two major cracks. **b** Details of the fracture surface stem from crack in **a** (see arrow)

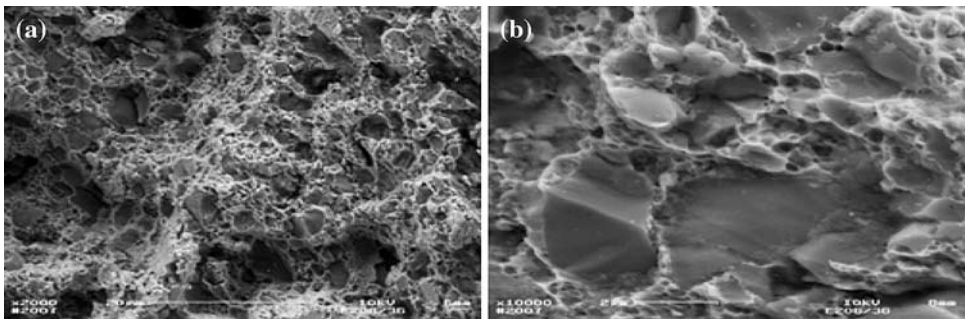

Fig. 11 SEM fractograph of the plate subjected to a plate impact

used, and it is not finally assured whether this phase is a boride or a carbide.

Quasistatic tensile tests show that the 0.2% yield strength and ultimate tensile strength are improved compared to the non-reinforced matrix alloy. Particle reinforcement reduces the elongation to failure compared to the non-reinforced matrix alloy.

Particle reinforcement augments the quasistatic compression strength more than the tensile strength. This effect is consistent with the behaviour of other reinforced metal systems such as Mg and Al alloys. The quasistatic compression strength is twice that of the tensile strength for the TiB2 particle-reinforced steel. The 316L MMC has an enormous quasistatic compression strength compared to the non-reinforced matrix alloy. The strain to failure amounts to 70% under the condition of a compression test due to the superposed hydrostatic pressure.

At high strain rate applied in the plate impact tests, both the compression and the tensile strength are increased.

The 316L MMC can suffer a high dynamic loading up to a strain to failure of about 45% without the MMC becoming brittle. The strain rate sensitivity of the MMC is small under dynamic loading. Metallographic investigation reveals that no adiabatic shearbanding of the MMC occurs.

Dynamic compression tests at elevated temperatures show relatively high dynamic compression strength when compared to the unreinforced 316 matrix.

Nitrogen-alloyed austenitic steels possess very high values of both tensile strength and compression strength, but the solid solution hardening effect of nitrogen decreases strongly with increasing temperature. These steels are low temperature alloys. The advantage in incorporating particles leads to an alloy with enhanced characteristics at elevated temperatures.

References

1. Lach E, Werner E, Bohmann A, Scharf M (2000) Adv Eng Mater 2(11):750–752
2. Uggowitzer PJ (1991) In: Speidel MO, Uggowitzer PJ (eds) Ergebnisse der Werkstoff-Forschung, vol 4. Thubal-Kain, Zürich
3. Kulikoxski Z, Wisbey A, Godfrey TMT, Goodwin PS, Flower HM (2000) Mater Sci Technol 925–928
4. Hopkinson J (1872) In: Proceedings of the Manchester literary and philosophical society, vol XI. pp 40–45
5. Lichtenberger A, Gazeaud G, Lach E (1988) In: International conference on mechanical and physical behaviour of materials under dynamic loading. Les Editions de Physique, Les Ulis, pp C3-589–594
6. Nahme H, Worswick MJ (1994) Dynamic properties and spall plane formation of brass, EURODYMAT 94, Oxford, UK, Sept. 26–30, pp 707–712
7. Kainer KU (1993) Advanced composites 93. In: Chandra T, Dhingra AK (eds) The minerals, metals & materials society, pp 1213–1219
8. Test Recommendation (1999) Dynamic compression testing using the split Hopkinson bar pressure bar. Dymat standardisation—identification n RE/002B/87, 2nd version
9. Lichtenberger A, Lach E, Bohmann A (1994) J Phys IV 4(8):29–34
10. Orowan E (1948) Symposium on internal stresses in metals and alloys, Institute of Metals, London, p 451
11. AMC Data, Iron & Steel MMC, Aerospace Metal Composites Limited, FARNBOROUGH, UK